A Balanced Mode Decomposition Approach for Equation-Free Reduced-Order Modeling of LPV Aeroservoelastic Systems

Andrea Iannelli *, Urban Fasel †, Nivethan Yogarajah ‡, Roy S. Smith §
Swiss Federal Institute of Technology, ETH Zürich, Zürich 8092, Switzerland

The paper proposes a novel approach to data-driven reduced-order modeling which combines the Dynamic Mode Decomposition technique with the concept of balanced realization. The information on the system comes from input, state, and output trajectories, and the goal is to derive a linear low-dimensional input-output model approximation. Since the dynamics of aerospace systems markedly changes when some parameters are varied, it is desirable to capture this feature in the system's description. Therefore, a Linear Parameter-Varying representation made of a collection of state-consistent linear time-invariant reduced-order models is sought. The main technical novelty of the proposed algorithm consists of replacing the orthogonal projection onto the POD modes, typical of Dynamic Mode Decomposition techniques, with a balancing oblique projection. The advantages are that the input-output information in the lower-dimensional representation is maximized, and that a parameter-varying projection is possible while also achieving state-consistency. The validity of the proposed approach is demonstrated on a morphing wing for airborne wind energy applications by comparing its prediction capabilities with those of a recent algorithm from the literature.

I. Introduction

THE use of data-driven methods to obtain low-order representations for complex systems described by high-dimensional and nonlinear (partial) differential equations has recently received great attention [1]. A common idea to many successful approaches is to project the high-dimensional data, typically consisting of system's trajectories, onto a lower dimensional subspace where the most important features of the dynamics are preserved. This is also the philosophy used in the Dynamic Mode Decomposition (DMD) technique [2], which, in its original formulation, computes the spectrum of a low-order linear dynamics approximating the training data. To achieve this, the method leverages the well-known reduction technique called Proper Orthogonal Decomposition (POD) [3]. The projecting subspace is indeed spanned by the left singular vectors (also termed POD modes) associated with the largest singular values of a snapshot matrix gathering the system's states at different measured times. Since the largest singular values are associated with the modes capturing most of the energy in the system, the orthogonal projection onto this lower dimensional subspace preserves the spatial structures with the highest energy content. However, there is no guarantee that this energy-based criterion is the optimal one to follow in every application. Moreover, for input-output model structures (e.g. the standard state-space models used to describe control systems), it is not clear whether a projection constructing with the POD modes, which only use state information, provide the best possible approximation.

Prompted by these observations, this paper investigates the use of data-driven (or equation-free) reduced-order modeling (ROM) techniques for aerospace applications where input-output models are sought, as it is the case for example in aeroservoelasticity. The state-of-the-practice in this field is to use well-established model-based reduction techniques [4]. However, the increasing complexity of the high-fidelity solvers on one hand, and the potential advantage of recalibrating or directly substituting parts of the code with experimental or flight data on the other, support the investigation of equation-free strategies. It is however important, to ensure their successful application, that distinctive aspects of these application domains are considered.

As mentioned earlier, a common feature of the most popular data-driven approaches is that they focus on internal dynamics (i.e. without external excitation and with fully observable states). The work in [5] recently extended the

*Postdoctoral Researcher, Automatic Control Lab, ETH Zürich, Switzerland (iannelli@control.ee.ethz.ch)
†Ph.D. Candidate, Laboratory of Composite Materials and Adaptive Structures, ETH Zürich, Switzerland, Member AIAA
‡M.Sc. Graduate student, ETH Zürich, Switzerland
§Professor, Automatic Control Lab, ETH Zürich, Switzerland, Associate Fellow AIAA

DMD framework to controlled systems (DMDc), but the key steps of the algorithm, included the computation of the projecting subspace, do not substantially change. Therefore, new methods should put emphasis on preserving the input-output behaviour of the system. In addition, it is very important to capture the variation of the system's properties (e.g. typically encountered in aeroservoelastic applications) as the operating conditions change. A natural framework to do this is the Linear Parameter-Varying (LPV) representation [6]. While LPV models are of acknowledged benefit for control related tasks [7–10], obtaining accurate models featuring low orders is notoriously a difficult task. One of the most common strategies is to seek low-order linear time-invariant (LTI) representations for a grid of frozen-parameter conditions and then, provided that state consistency holds across the family of models, interpolate them for varying parameters [11]. An algorithm that applies this strategy in the data-driven setting by following a DMD approach was proposed in [12] under the name of input-output reduced-order model (IOROM) method. In DMD-based approaches, interpolating local LTI models can be however in principle problematic, since state consistency will depend on the selection of the projecting subspace. If this changes across the parameter range, as it is the case if one computes the POD modes at each grid point, then state consistency will not hold in general and thus the LPV representation is not achieved. Conversely, if the subspace is kept fixed for all the frozen-parameter LTIs, then accuracy might deteriorate since projection will no more take place onto the subspace associated with the POD for the considered parameter.

Motivated by the discussion above, this work proposes a novel equation-free approach for obtaining LPV low-order models. The idea to address the aforementioned issues is to use, instead of an orthogonal projection associated with one subspace, an oblique projection. This is associated with two subspaces, a basis space and a test space, characterizing the range space and null space of the projection, respectively. Oblique projection, which is a tool employed in model reduction [13] and system identification [14], was previously used in the context of model-based reduction of LPV models in [15]. The oblique projection is instead used here for the first time, to the best of the authors' knowledge, in the context of DMD-type data-driven ROM approaches as an alternative choice to the subspace spanned by the POD modes. After describing the steps of the Balanced Mode Decomposition (BMD) algorithm, its performance is compared with a recent extension of the DMD with control algorithm. Precisely, the algebraic DMDc (aDMDc) algorithm was proposed in [16] to extend DMDc to the case of parameters' variation and to systems described by algebraic, besides differential, equations. Including algebraic constraints is indeed very important when considering state trajectories generated by aerodynamic solvers capturing unsteady effects, such as in panel methods or unsteady vortex lattice methods [17].

The algorithms are tested on a high-fidelity, fluid-structure interaction (FSI) numerical model of an airborne wind energy (AWE) morphing wing. The FSI simulator is described in [18] and the wing was analyzed in detail in [19].

II. Equation-free low-order modeling

This section provides some background on equation-free ROM algorithms. In Section II.A the general data-driven low-order modeling problem is presented. Section II.B reviews then the algebraic DMD with Control (aDMDc) [16], an equation-free ROM algorithm from the literature used for comparison in the result section.

A. Problem statement and preliminaries

The starting point is a generic discrete-time nonlinear parameter-varying model which can be used to describe typical aeroservoelastic systems modelled by FSI solvers:

$$\begin{aligned} x_{k+1} &= f(x_k, u_k, \rho_k), \\ y_k &= h(x_k, u_k, \rho_k), \end{aligned} \tag{1}$$

where $x \in \mathbb{R}^{n_x}$, $u \in \mathbb{R}^{n_u}$, $y \in \mathbb{R}^{n_y}$ are the state, input and output, and $\rho : \mathbb{R} \to \mathbb{R}^{n_\rho}$ is a vector of time-varying parameters defining the operating conditions of the system. The problem of finding an LPV low-order approximation of (1) can be divided into two phases: first, LTI approximations for frozen values of ρ in a pre-defined grid $\{\rho^j\}_{j=1}^{n_g}$ are computed; then, an LPV model is obtained through appropriate interpolation.

It is assumed that for each frozen value $\bar{\rho}$ there exists an equilibrium point characterized by the tuple $(\bar{x}(\bar{\rho}),\bar{u}(\bar{\rho}),\bar{y}(\bar{\rho}))$ such that:

$$\begin{aligned} \bar{x}(\bar{\rho}) &= f(\bar{x}(\bar{\rho}), \bar{u}(\bar{\rho}), \bar{\rho}), \\ \bar{y}(\bar{\rho}) &= h(\bar{x}(\bar{\rho}), \bar{u}(\bar{\rho}), \bar{\rho}). \end{aligned}$$

The deviation vectors $\tilde{x}_k := x_k - \bar{x}(\bar{\rho})$, $\tilde{u}_k := u_k - \bar{u}(\bar{\rho})$, and $\tilde{y}_k := y_k - \bar{y}(\bar{\rho})$ are then used to express the LTI

approximation of the system around the equilibrium in state-space form as:

$$\tilde{x}_{k+1} = A(\bar{\rho})\tilde{x}_k + B(\bar{\rho})\tilde{u}_k, \tag{2a}$$
$$\tilde{y}_k = C(\bar{\rho})\tilde{x}_k + D(\bar{\rho})\tilde{u}_k, \tag{2b}$$

where $(A(\bar{\rho}),B(\bar{\rho}),C(\bar{\rho}),D(\bar{\rho}))$ represent the linearization around the considered trim point associated with $\bar{\rho}$ (the dependence on the objects on a fixed value of the parameter ρ will be dropped in the remainder when clear from the context).

In the data-driven setting, the only information on the system comes from input, state, and output trajectories $\{x_k, u_{k-1}, y_{k-1}\}_{k=1}^{n_s}$ of length n_s, and is gathered in the following snapshot matrices:

$$\begin{aligned}
X_0 &= \begin{bmatrix} x_0 - \bar{x} & x_1 - \bar{x} & \dots & x_{n_s-1} - \bar{x} \end{bmatrix} && \in \mathbb{R}^{n_x \times n_s}, \\
X_1 &= \begin{bmatrix} x_1 - \bar{x} & x_2 - \bar{x} & \dots & x_{n_s} - \bar{x} \end{bmatrix} && \in \mathbb{R}^{n_x \times n_s}, \\
U_0 &= \begin{bmatrix} u_0 - \bar{u} & u_1 - \bar{u} & \dots & u_{n_s-1} - \bar{u} \end{bmatrix} && \in \mathbb{R}^{n_u \times n_s}, \\
U_1 &= \begin{bmatrix} u_1 - \bar{u} & u_2 - \bar{u} & \dots & u_{n_s} - \bar{u} \end{bmatrix} && \in \mathbb{R}^{n_u \times n_s}, \\
Y_0 &= \begin{bmatrix} y_0 - \bar{y} & y_1 - \bar{y} & \dots & y_{n_s-1} - \bar{y} \end{bmatrix} && \in \mathbb{R}^{n_y \times n_s}.
\end{aligned} \tag{3}$$

The notation $[X_0;\ \ U_0]$ will denote the operation of stacking row-wise two matrices X_0 and U_0.

The first goal is to obtain a low-order and linear time-invariant approximation of (2), that is:

$$\begin{aligned}
\tilde{z}_{k+1} &= F\tilde{z}_k + G\tilde{u}_k, \\
\tilde{y}_k &= H\tilde{z}_k + D\tilde{u}_k,
\end{aligned}$$

where $\tilde{z} \in \mathbb{R}^{n_z}$ and $n_z \ll n_x$. Once this is available, the response of the system at any value ρ_k for a generic time-varying trajectory of the parameter is obtained via interpolation. For control application, it is desirable to perform this at matrix level by directly interpolating the family of frozen LTI systems. However, this requires state-consistency across the parameters range and when this is not achieved one can interpolate the signals of interest instead. An example of the latter solution is the aDMDc algorithm, reviewed next.

B. Algebraic Dynamic Mode Decomposition with Control algorithm

The algebraic Dynamic Mode Decomposition with Control (aDMDc) algorithm was recently proposed in [16] to extend the DMDc algorithm to systems described by algebraic-differential equations. The DMDc algorithm from [5] is first briefly reviewed. This algorithm seeks a data-driven approximation of the matrices involved in the state equation (2) by means of two truncated singular value decompositions (SVD) of the snapshot matrices. The first one is:

$$[X_0;\ \ U_0] = U\Sigma V^\top \cong U_r \Sigma_r V_r^\top, \tag{4}$$

where the subscript r denotes a truncation of the SVD decomposition of order r (obtained by retaining only the r largest singular values in the decomposition). Note that the value of r has nothing to do in principle with the size of the final reduced-order model, and it could be set for example by using the hard threshold criterion suggested in [20]. The effect of choosing r on the accuracy of the model will be discussed in the result section. The second one is computed from the snapshot matrix X_1:

$$X_1 = \hat{U}\hat{\Sigma}\hat{V}^\top \cong \hat{U}_{n_z}\hat{\Sigma}_{n_z}\hat{V}_{n_z}^\top, \tag{5}$$

where the columns of $\hat{U}_{n_z}$ provides the set of POD modes used for the projection on a lower dimensional space, and the selection of n_z fixes the size of the reduced-order model.

An approximation of the high-order matrices appearing in (2) can be formulated in terms of the truncated SVD (4) and the snapshot matrix X_1 as:

$$[A\ \ B] = X_1 V_r^\top \Sigma_r^{-1} U_r^\top. \tag{6}$$

Then, a low-order approximation is obtained by projecting (6) onto the set of POD modes by making use of (5):

$$[F \;\; G] = \left[\hat{U}_{n_z}^\top A \hat{U}_{n_z} \quad \hat{U}_{n_z}^\top B\right].$$

Therefore, the sought low-order model is:

$$\tilde{z}_{k+1} = F\tilde{z}_k + G\tilde{u}_k,$$

where the high-order state can be recovered as $\tilde{x} = \hat{U}_{n_z}\tilde{z}$.

The aDMDc builds on the DMDc approach and addresses the presence of algebraic constraints in the dynamic equations which might arise when considering unsteady aerodynamics features. Specifically, the FSI model employed in [16] implements a 3D panel with wake's features inspired by the method in [17], which leads to a dependence of the states evolution on the inputs at the next time step. Therefore, a slightly different starting point from the general one presented in (1) has to be considered, namely:

$$\begin{aligned} g(x_{k+1}, u_{k+1}) &= f(x_k, u_k, \rho_k), \\ y_k &= h(x_k, u_k, \rho_k), \end{aligned} \tag{7}$$

where g is in general a nonlinear function taking into account the dependence of the states on the control inputs at the next time step. This dependence results from algebraic equations relating the doublet strengths (aerodynamics states) and downwash (function of the other states and the control inputs). While this effect is sometimes accounted for with artificial aerodynamic states by simply changing the feedtrough matrix to the outputs, to correctly capture the evolution of the states it is important to consider the problem as stated in (7). The reader is referred to [16] for further discussion on this aspect.

The LTI representation proposed in aDMDc to account for the algebraic constraints due to the unsteady aerodynamics is thus:

$$\tilde{x}_{k+1} = A\tilde{x}_k + B\tilde{u}_k + R\tilde{u}_{k+1},$$

where, as in DMDc, the objective is to find a low-order approximation for the state equation only. The only difference with DMDc is that now the first SVD decomposition is computed with respect to the snapshot matrices X_0, U_0, and U_1, that is:

$$[X_0; \;\; U_0; \;\; U_1] = U\Sigma V^\top \cong U_r \Sigma_r V_r^\top.$$

And the high-order matrices are thus approximated as:

$$[A \;\; B \;\; R] = X_1 V_r^\top \Sigma_r^{-1} U_r^\top.$$

The second truncated SVD (4) instead is unchanged, and a low-order approximation is then obtained by projecting (6) onto the same set of POD modes used in DMDc:

$$[F \;\; G \;\; L] = \left[\hat{U}_{n_z}^\top A \hat{U}_{n_z} \quad \hat{U}_{n_z}^\top B \quad \hat{U}_{n_z}^\top R\right].$$

This procedure results in the aDMDc low-order model:

$$\tilde{z}_{k+1} = F\tilde{x}_k + G\tilde{u}_k + L\tilde{u}_{k+1}, \tag{8}$$

where the high-order state can again be obtained from $\tilde{x} = \hat{U}_{n_z}\tilde{z}$.

The approach proposed in [16] to handle parameters variations is to use a different set of POD modes for each value of ρ in the grid. As a result, the frozen LTI models (8) do not have a consistent basis for the state, and thus the signals, instead of the matrices, are directly interpolated. That is, the frozen LTI models (8) are simulated simultaneously, the relative states are lifted to the high-order ones using the corresponding projection matrices (e.g. $\hat{U}_{n_z}(\rho^j)$ for the model corresponding to the $j-th$ element in the parameter space), and the state corresponding to the desired value of ρ is obtained by interpolating the high-dimensional states. While this approach has in principle the advantage of projecting over POD modes specifically computed for a particular value of ρ, it also means that an LPV model is not available. This for example precludes the use of LPV robust control design strategies [9]. While other control techniques, such as model predictive control, can still be successfully used [16], this will entail running in parallel multiple models (8).

III. Balanced Mode Decomposition with oblique projection

This section presents the main technical aspects of the Balanced Mode Decomposition (BMD) algorithm. Section III.A presents the algorithm and Section III.B gives more details on the selection of the two subspaces defining the projection. Finally, Section III.C presents a version of the algorithm which accounts for algebraic constraints and can thus be used to analyze the morphing wing in Section IV.

A. Formulation of the algorithm

The frozen-parameter case is considered first, leveraging the interpretation of DMD as linear dynamics fitting [21]. Specifically, given the snapshot matrices (3), the state-space matrices (A, B, C, D) defining (2) can be in principle obtained by solving the following least-squares problem:

$$\min_{A,B,C,D} \left\| \begin{bmatrix} X_1 \\ Y_0 \end{bmatrix} - \begin{bmatrix} A & B \\ C & D \end{bmatrix} \begin{bmatrix} X_0 \\ U_0 \end{bmatrix} \right\|_F^2, \tag{9}$$

where the subscripts F denotes the Frobenius norm of a matrix. Naturally, simply solving (9) does not provide a low-dimensional representation of the system because the identified state space model (A,B,C,D) is of order n_x. To achieve this, the conventional approach in DMD, recently extended in [12] to the input-output setting with the *IOROM* method, is to project the state orthogonally onto a low-dimensional subspace of dimension n_z. This is done by introducing the projection matrix $Q \in \mathbb{R}^{n_x \times n_z}$, where $Q^\top Q = I_{n_z}$, such that the orthogonal projection of $\tilde{x}$ on an n_z-dimensional subspace reads as $QQ^\top \tilde{x}$. Equivalently, one can think that the original state is approximated by $\tilde{x} \cong Q\tilde{z}$ for some coefficient vector $\tilde{z} \in \mathbb{R}^{n_z}$. It then follows that the vector $\tilde{z} = Q^\top \tilde{x} \in \mathbb{R}^{n_z}$ is the state of the following low-order approximation of (2):

$$\begin{bmatrix} A & B \\ C & D \end{bmatrix} \approx \begin{bmatrix} QFQ^\top & QG \\ HQ^\top & D \end{bmatrix} = \begin{bmatrix} Q & 0 \\ 0 & I_{n_y} \end{bmatrix} \begin{bmatrix} F & G \\ H & D \end{bmatrix} \begin{bmatrix} Q^\top & 0 \\ 0 & I_{n_u} \end{bmatrix}.$$

The standard choice is to use the POD modes of X_0 to construct the projection matrix Q, namely:

$$\begin{aligned} X_0 &\cong U_{n_z} \Sigma_{n_z} V_{n_z}^\top, \\ Q &= U_{n_z}, \end{aligned} \tag{10}$$

where U_{n_z} contains the left singular vectors associated with the n_z largest singular values of X_0.

In this work, a different strategy is employed to project the data. Precisely, the orthogonal projection is replaced by an oblique projection. Given $V \in \mathbb{R}^{n_x \times n_z}$, and $W \in \mathbb{R}^{n_x \times n_z}$, such that W is bi-orthogonal to V, i.e. $W^\top V = I_{n_z}$, an oblique projection can be defined by the matrix $\Pi = VW^\top$. That is, the oblique projection of $\tilde{x}$ reads as $VW^\top \tilde{x}$. Equivalently, one can think that the original state is approximated by $\tilde{x} \cong V\tilde{z}$ (where, as before, $\tilde{z} \in \mathbb{R}^{n_z}$ is some coefficient vector), and the component of $\tilde{x}$ that is eliminated by the projection is in the nullspace of Π (or, equivalently, it is orthogonal to W). As opposed to the orthogonal projection, which is characterized by a single subspace (the one spanned by the columns of Q), the oblique projection is thus defined by two subspaces: the basis space (spanned by the columns of V), such that the projection of $\tilde{x}$ lies in the span of V; and the test space (spanned by the columns of W), such that the projection $V\tilde{z}$ has zero error within it, i.e. $W^\top (\tilde{x} - Vz) = 0$. This is the feature that enables the BMD algorithm to obtain families of LTI systems having state-consistency and characterized by parameter-varying projections. Indeed, it is sufficient to employ a fixed V (since this defines the state basis) and a parameter-dependent W.

This approach leads to the following low-order approximation of (2):

$$\begin{bmatrix} A & B \\ C & D \end{bmatrix} \approx \begin{bmatrix} VFW^\top & VG \\ HW^\top & D \end{bmatrix} = \begin{bmatrix} V & 0 \\ 0 & I_{n_y} \end{bmatrix} \begin{bmatrix} F & G \\ H & D \end{bmatrix} \begin{bmatrix} W^\top & 0 \\ 0 & I_{n_u} \end{bmatrix}, \tag{11}$$

where the basis V and test spaces W are computed from data in order to maximize the input-output content captured in the projection (as detailed in Section III.B). The matrices (F,G,H,D) can then be obtained with the following least-squares problem:

$$\min_{F,G,H,D} \left\| \begin{bmatrix} X_1 \\ Y_0 \end{bmatrix} - \begin{bmatrix} V & 0 \\ 0 & I_{n_y} \end{bmatrix} \begin{bmatrix} F & G \\ H & D \end{bmatrix} \begin{bmatrix} W^\top & 0 \\ 0 & I_{n_u} \end{bmatrix} \begin{bmatrix} X_0 \\ U_0 \end{bmatrix} \right\|_F^2, \tag{12}$$

which has solution:

$$\begin{bmatrix} F & G \\ H & D \end{bmatrix}_{opt} = \begin{bmatrix} W^\top X_1 \\ Y_0 \end{bmatrix} \begin{bmatrix} W^\top X_0 \\ U_0 \end{bmatrix}^\dagger . \tag{13}$$

where † denotes the pseudo-inverse of a matrix.

To build a low-order LPV model, snapshot matrices are first collected for different realizations of $\{\rho^j\}_{j=1}^{n_g}$, and the least-squares problem (12) is solved at each grid point. Crucially, the test space W is allowed to be a function of ρ, as motivated previously. This leads to the following solution for the matrices on the pre-defined grid.

$$\begin{bmatrix} F(\rho^j) & G(\rho^j) \\ H(\rho^j) & D(\rho^j) \end{bmatrix}_{opt} = \begin{bmatrix} W^\top(\rho^j) X_1(\rho^j) \\ Y_0(\rho^j) \end{bmatrix} \begin{bmatrix} W^\top(\rho^j) X_0(\rho^j) \\ U_0(\rho^j) \end{bmatrix}^\dagger . \tag{14}$$

The BMD LPV reduced-order model is then obtained by interpolating the frozen matrices (14) across the parameter's range:

$$\begin{aligned} \tilde{z}_{k+1} &= F_{\rho_k} \tilde{z}_k + G_{\rho_k} \tilde{u}_k + (\bar{z}(\rho_k) - \bar{z}(\rho_{k+1})), \\ \tilde{y}_k &= H_{\rho_k} \tilde{z}_k + D_{\rho_k} \tilde{u}_k . \end{aligned} \tag{15}$$

where $(F_\rho, G_\rho, H_\rho, D_\rho)$ are obtained by interpolating the corresponding matrices at the query value ρ_k, and $\bar{z}(\rho_k) = W^\top \bar{x}(\rho_k)$. The term $(\bar{z}(\rho_k) - \bar{z}(\rho_{k+1}))$, which did not appear in 8, is proposed here to take into account the fact that the equilibrium point associated with each ρ is in general different.

A pseudoalgorithm of the BMD algorithm is given in the next section, after having discussed the computation of basis and test spaces.

B. Basis and test spaces construction

The interpolation of the frozen reduced-order models can be done in (15) at the state-matrices level, as opposed to what is the case for aDMDc. While this favourable property was also achieved by other DMD-inspired methods, such as the IOROM algorithm proposed in [12], the price to pay to guarantee state consistency was that a fixed projection matrix for all frozen models had to be used. Thanks to the use of a parameter-varying test space $W(\rho)$, the projection can be made here also parameter-dependent, with the clear advantage that the subspaces where states are projected can be computed anew for each value of the parameters.

The other motivation for the proposal of the BMD algorithm has to do with the fact the projecting onto the subspace spanned by the POD modes can be arbitrary suboptimal, because they are selected only based on the energy in the measured states. In the input-output context, a subspace typically providing lower input-output errors with respect to the others having same size n_z is the one where the system's state is in balanced coordinates [22]. This is indeed the principle behind balanced truncation, which consists of removing the states corresponding to the smallest $n_x - n_z$ Hankel singular values. This is an effective heuristic justified by the fact that their sum provides a lower bound and, for systems in balanced coordinates, an upper bound on the quality of the approximation achieved by removing system's states [4, 23].

These control theoretic properties are used here to select the basis and test spaces. Specifically, V and W are computed from the *empirical* controllability and observability Gramians of the system, respectively W_c and W_o. This ensures that the projection preserves the most observable and controllable states, enabling an approximate model-free balanced truncation of the reduced-order LPV model.

Because a model of the system is not available, empirical Gramians are computed from appropriate input and output trajectories of the system. The empirical controllability Gramian can be obtained by impulse response simulations (one for each input channel). If the high-fidelity model is linear and its adjoint is available, then the empirical observability Gramian can be computed by impulse response simulations (one for each output channel) of the adjoint system, as in balanced POD [3]. Otherwise, the approach developed in [24], valid also for nonlinear systems and not requiring an adjoint model, can be used. The main disadvantage is that it requires one simulation for each state. Specifically, the initial condition of each state is perturbed and the corresponding response (for zero input) simulated. Since these are unforced responses, the simulation time before the output decays depends on the dominant poles. When the system is sufficiently damped, it will be generally sufficient to observe only the initial time-steps and thus this calculation can be efficiently implemented to overcome costly simulations.

Once W_c and W_o are available, the procedure proposed in [15] to compute an oblique projection for given controllability and observability Gramians is employed to construct the test and basis spaces. This consists of a series

of singular value and QR decompositions and is reported in the first part of the pseudocode below (where MATLAB notation is used for matrix operations), which summarizes the main steps involved in the BMD algorithm.

Algorithm 1 Balanced Mode Decomposition with oblique projection

Input: parameter grid points $\{\rho^j\}_{j=1}^{n_g}$; snapshot matrices $\{X_0(\rho^j), X_1(\rho^j), U_0(\rho^j), Y_0(\rho^j)\}_{j=1}^{n_g}$; empirical Gramians $\{W_c(\rho^j), W_o(\rho^j)\}_{j=1}^{n_g}$; model desired order n_z.

Output: reduced-order models at the grid points $\{F(\rho^j),G(\rho^j),H(\rho^j),D(\rho^j)\}_{j=1}^{n_g}$; test space projection matrices $\{W(\rho^j)\}_{j=1}^{n_g}$; fixed basis space projection matrix V.

for $j = 1, ..., n_g$ **do**
  $L_c(\rho^j)L_c(\rho^j)^\top = W_c(\rho^j)$ Cholesky factorization of W_c
  $L_o(\rho^j)L_o(\rho^j)^\top = W_o(\rho^j)$ Cholesky factorization of W_o
  $(U, \star, \star) = \text{svd}(L_c(\rho^j)^\top L_o(\rho^j))$
  $(\bar{U}, \star, \star) = \text{svd}(L_c(\rho^j)U(:, 1 : n_z))$
  $\bar{Q}(:, 1 + n_z(j-1) : n_z j) = \bar{U}(:, 1 : n_z)$
end for
$(Q, \star, \star) = svd(\bar{Q})$
$V = Q(:, 1 : n_z)$
for $j = 1, ..., n_g$ **do**
  $(Q, R) = qr(L_o(\rho^j)^\top V)$ Thin QR factorization
  $Q = Q(:, 1 : n_z)$
  $R = R(1 : n_z, :)$
  $W(\rho^j) = L_o(\rho^j)Q(R^\top)^{-1}$ Time-varying test space

$$\begin{bmatrix} F(\rho^j) & G(\rho^j) \\ H(\rho^j) & D(\rho^j) \end{bmatrix} = \begin{bmatrix} W^\top(\rho^j)X_1(\rho^j) \\ Y_0(\rho^j) \end{bmatrix} \begin{bmatrix} W^\top(\rho^j)X_0(\rho^j) \\ U_0(\rho^j) \end{bmatrix}^\dagger \quad \text{BMD regression problem}$$

end for

The output $\{F(\rho^j),G(\rho^j),H(\rho^j),D(\rho^j)\}_{j=1}^{n_g}$ provided by the BMD algorithm is a grid LPV model. After an interpolation algorithm to evaluate the matrices' entries for any value of ρ inside the considered range has been chosen, this model can be used for simulation and control design. Note also that recently proposed robust analysis methods for linear-time varying (LTV) systems [25, 26] can be applied to investigate different aircraft manoeuvres (fixing a particular trajectory for ρ transforms the LPV into an LTV system). The parameter-varying test space $W(\rho^j)$ can be useful to gain insights into the aeroeservoealstic modes which have been eliminated and those that have been kept in the projection, while the parameter-independent basis space can be used to recover at each time-step k the high-dimensional state via the transformation $\tilde{x}_k = V\tilde{z}_k$. The construction of the basis and test spaces given above, together with Eqs. (11)-(13) illustrated in the previous section, explain the reason for the name Balanced Mode Decomposition. Indeed, the proposed algorithm can be seen as a version of the classic DMD technique for the reconstruction of a state-space model where the orthogonal projection onto the POD modes is replaced by an oblique projection defined by the balancing and adjoint modes of the system, leading to a balanced decomposition.

It is finally noted that, as said in the beginning, the algorithm provides an approximate balanced truncation. Approximation is related to the use of empirical Gramians, which are only finite-time approximations of the true ones (for this reason, also called finite-time Gramians) since their computation is trajectory-based. As a result, they only provide in principle a finite-time balanced realization [4], while the theoretical order reduction error bounds are only available for infinite-time balanced realizations. This source of error can however be made arbitrarily small by using for constructing the Gramians long enough data sequences, such that the response of the system has decayed.

C. Extension to handle algebraic constraints

The BMD algorithm will be applied in Section IV to the FSI solver developed in [18], which presents the algebraic constraints described in Section II.B. It is thus presented here an extension of the algorithm discussed in the previous

section to handle this instance. For a fixed value of ρ, the model structure for the high-order model becomes:

$$\begin{aligned} \tilde{x}_{k+1} &= A\tilde{x}_k + B\tilde{u}_k + R\tilde{u}_{k+1}, \\ \tilde{y}_k &= C\tilde{x}_k + D\tilde{u}_k + P\tilde{u}_{k+1}, \end{aligned}$$

where a potential effect of the algebraic constraints in the output equation is also considered via the matrix P. Therefore, the low-order approximation becomes now:

$$\begin{bmatrix} A & B & R \\ C & D & P \end{bmatrix} \approx \begin{bmatrix} VFW^\top & VG & VL \\ HW^\top & D & P \end{bmatrix} = \begin{bmatrix} V & 0 \\ 0 & I_{n_y} \end{bmatrix} \begin{bmatrix} F & G & L \\ H & D & P \end{bmatrix} \begin{bmatrix} W^\top & 0 & 0 \\ 0 & I_{n_u} & 0 \\ 0 & 0 & I_{n_y} \end{bmatrix}.$$

The new objective function to be minimized is:

$$\min_{F,G,L,H,D,P} \left\| \begin{bmatrix} X_1 \\ Y_0 \end{bmatrix} - \begin{bmatrix} W & 0 \\ 0 & I_{n_y} \end{bmatrix} \begin{bmatrix} F & G & L \\ H & D & P \end{bmatrix} \begin{bmatrix} W^\top & 0 & 0 \\ 0 & I_{n_u} & 0 \\ 0 & 0 & I_{n_y} \end{bmatrix} \begin{bmatrix} X_0 \\ U_0 \\ U_1 \end{bmatrix} \right\|_F^2,$$

and the new optimal solution is:

$$\begin{bmatrix} F & G & L \\ H & D & P \end{bmatrix} = \begin{bmatrix} W^\top X_1 \\ Y_0 \end{bmatrix} \begin{bmatrix} W^\top X_0 \\ U_0 \\ U_1 \end{bmatrix}^\dagger. \tag{16}$$

IV. Results

This section presents and discusses results obtained from the application of the aDMDc and BMD algorithms to the flexible and highly cambered morphing wing depicted in Fig. 1. The wing is made of composite material, and the trailing edges are able to morph and, by doing so, to increase or decrease the camber, thus replacing conventional ailerons. The reader is referred to the related previous works for details on the wing design [27] and its investigation with FSI tools [19].

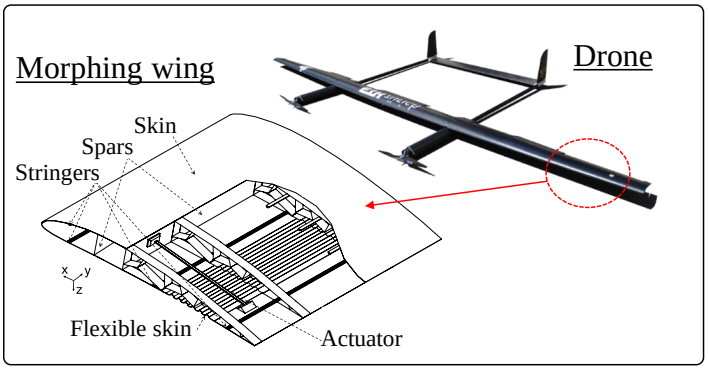

Fig. 1 Illustrative depiction of the aeroeservoelastic testcase [19].

The state of the system x consists of the total number of structural modes of the wing (extracted from the commercial software Nastran [28]) and the doublet strengths (from the 3D panel method solver), with $n_x = 618$. The input vector u of size $n_u = 6$ is given by:

$$u = [\alpha;\ \ p;\ \ q;\ \ r;\ \ F_s;\ \ F_{as}], \tag{17}$$

where α is the angle of attack, p, q, and r are the roll, pitch, and yaw rotation rates and F_s and F_{as} are the symmetric and anti-symmetric morphing actuation inputs. Unless otherwise specified, we will consider here as output only the first bending mode of the wing ($n_y = 1$), since this is usually the one associated with dynamic instabilities and

large deformations, and thus it is of especial interest for active control tasks. The flight speed will be considered as time-varying parameter ($n_\rho = 1$). These analyses choices are done here for the sake of simplicity, since the algorithms can be applied to a generic number of outputs and varying parameters.

The training phase, common to all the algorithms and consisting of generating the snapshot matrices in Eq. (3), is carried out in the same way as described in [16]. Specifically, the system is excited with impulses in the input channels deployed in random order, and trajectories of length $n_s = 500$ with sampling time $0.006s$ are recorded.

A. Fixed-parameter models

In this first set of tests, the accuracy of the models at fixed values of the flight speed V is assessed. The models are simulated using sinusoidal inputs in each input channel, choosing the same values tested in [16]. The frequencies, different for each channel, are all of the order of magnitude of the aircraft reduced frequency $\omega_r =: \frac{V}{\bar{c}}$, where $\bar{c}$ is the mean chord of the wing. This test is performed for 3 flight speeds in the range of operating conditions of interest, namely V=30 $\frac{m}{s}$, V=40 $\frac{m}{s}$, and V=50 $\frac{m}{s}$. To quantify the accuracy as a function of the order of the model n_z, the Euclidean norm of the error signal between the first bending mode amplitude provided by the high-fidelity FSI and the prediction obtained with the three ROM algorithm is computed. It is also noted that the results obtained with the aDMDc algorithm showed great sensitivity, in the range of n_z displayed in Fig. 2, to the SVD truncation order r employed in Eq. (4). Using the hard threshold criterion from [20] was not satisfactory as it resulted in a very large r (therefore the truncation included very low singular values deteriorating the approximation). A fine-tuning of r proved to be necessary to obtain acceptable results, and therefore, to present an objective analysis, unless otherwise specified it is used $r = n_z$.

Results are shown in Fig. 2.

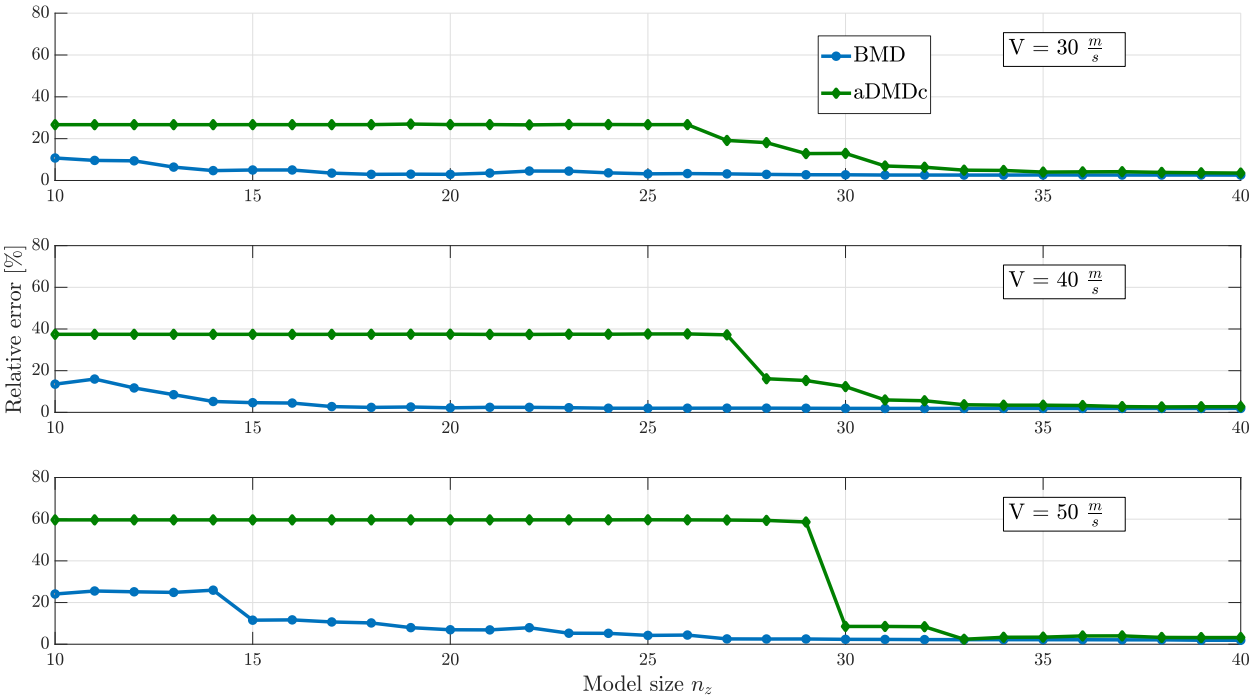

Fig. 2 Error on the prediction of the wing's bending mode made by the two algorithms for three different values of the flight speed.

It is clear that for all speeds BMD provides the smallest error for low order approximation of the full dynamics, as expected in view of the optimized choice of low-dimensional subspace where the high-dimensional data are projected. As the size n_z of the system increases, the difference between the algorithms is less noticeable and, for high enough orders, the algorithms tend to give same results.

B. Parameter-varying models

In the second set of tests, the accuracy during parameter-varying manoeuvres is tested. The reduced-order models are obtained using snapshot matrices obtained gridding the flight speed range every 2 $\frac{m}{s}$.

1. Response to sinusoidal excitation

The same sinusoidal excitation signals used in Section IV.A are considered here, and a manoeuvre of $3s$ where the flight speed linearly increases from V=20 $\frac{m}{s}$ to V=50 $\frac{m}{s}$ is analyzed. Thus, a grid of 16 different speeds ($n_g = 16$) is considered. In Fig. 3, the bending mode amplitude response obtained with the FSI solver (*FSI*) is compared with the predictions of the two algorithms when the order of the models is fixed at $n_z = 14$. All the signals are normalized by the largest value of the bending amplitude measured in the FSI simulation. The aDMDc model was here obtained by fine tuning the threshold value r in order to provide the best results. Indeed, in the low order regime for the currently considered parameter-varying case, the choice $r = n_z$ gave rise in some cases to unstable models.

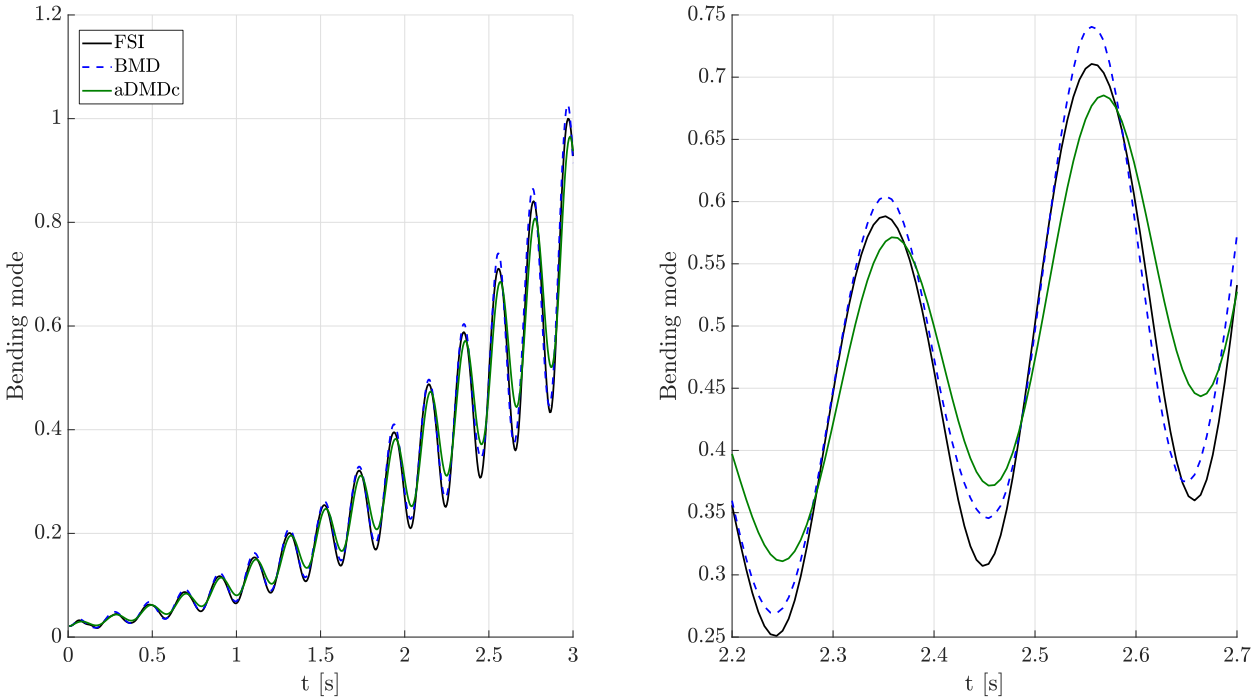

Fig. 3 Comparison of the normalized output (bending mode) of the low-order models with $n_z = 14$ against the FSI solver for parameter-varying simulations.

The plot confirms, also in the LPV setting, that the BMD algorithm guarantees the smallest error when a low-order approximation of the system is desired. It is remarked that aDMDc does not provide a family of interpolated low-order models, but instead requires to interpolate directly the high-order states, thus simulations in parallel of the low-order models are needed. The better performance of BMD, despite the fact that a part of the projection (the one related to the basis space) is constant, is ascribed to the improved selection of subspace for the projection compared to the standard POD one. In addition to the improvement in the accuracy, the BMD algorithm is also capable of providing a family of consistent LTI models with the discussed advantages for control design, not further investigated in this work.

It is then investigated the capability of the models to predict other quantities of interest, such as for example aerodynamic coefficients depending on the system's states. In particular, we test here the accuracy when these coefficients are computed directly from the states. That is, the low-order states are lifted to the high-order ones, which are then used to compute the coefficients using their functional dependence on the states. While this is the only possible way of reconstructing system's signals for aDMDc, in BMD this can alternatively be done by simply adding the desired quantities to the vector of output (as already done for the bending mode amplitude before) and generating new reduced-order models. This would probably be the preferred approach if the signals are used for control (either because they represent measurements fed to the controller or because they are performance to be optimized), but from a

modeling perspective it is also of interest the characterization analyzed here.

Figure 4 shows the normalized lift, pitch, and drag coefficients for the same constantly accelerated manoeuvre considered so far and with sinusoidal excitation. Normalization is performed, as done earlier in Figure 3, by dividing each signal by the largest value of the corresponding signal in the FSI simulation. The models have size $n_z = 14$. The shown aDMDc model was here obtained by fine tuning the threshold value r.

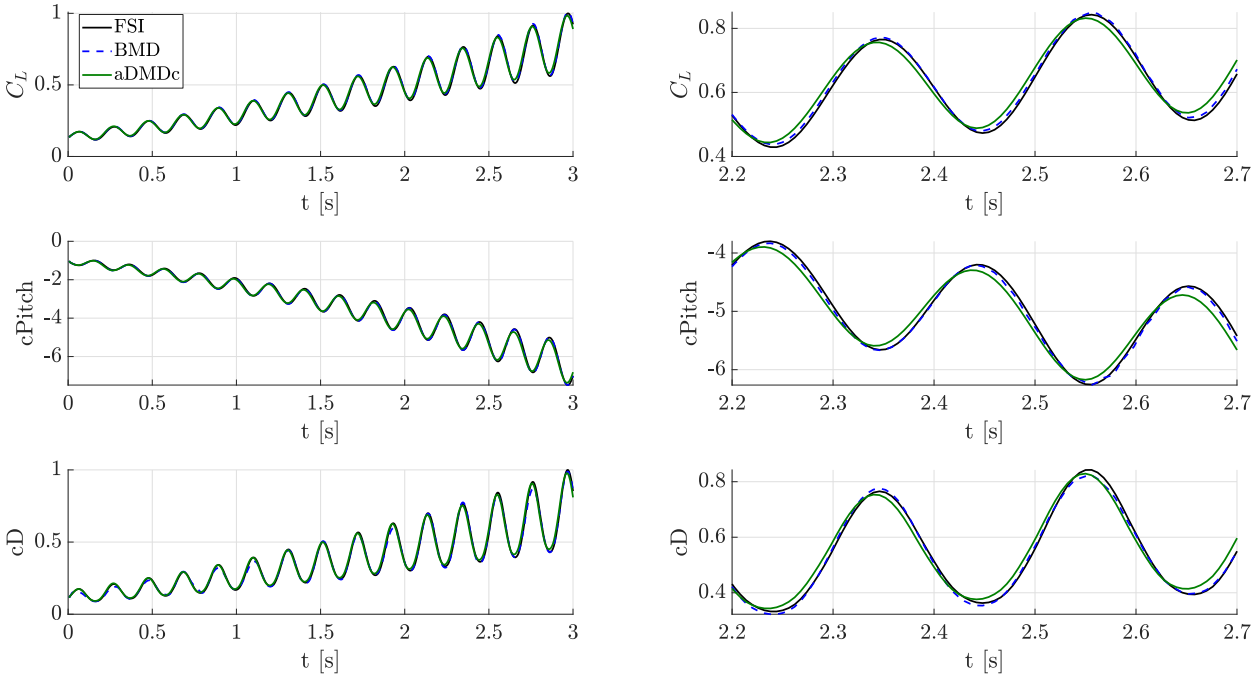

Fig. 4 Comparison of the normalized lift, pitch, and drag coefficients for a parameter-varying simulation with $n_z = 14$ and sinusoidal inputs.

The same observations gathered earlier with respect to the trajectory of the bending mode (Figure 4) are confirmed here. It is particularly interesting to observe that, even though these coefficients are not output of the model, and thus the balancing projection is not aimed directly at capturing them, the BMD algorithm is still able to perform better than aDMDc.

2. Simulation accuracy for different input signals

This section investigates the accuracy of the reduced-order models for different types of input signals. The Euclidean norm of the error signal between the first bending mode amplitude provided by the high-fidelity FSI and the prediction obtained with the three ROM algorithm is again used as metric to assess the quality of the approximation. The manoeuvre considered here is the same analyzed in Section IV.B.1, that is constant acceleration from V=20 $\frac{m}{s}$ to V=50 $\frac{m}{s}$ in $3s$. Three classes of inputs are considered: *Sine* coincides with the signal tested so far and already investigated in [16]; *Chirp* excites the system by injecting in all 6 input channels defined in (17) a chirp signal with frequency linearly varying from $0.1\omega_r$ to ω_r; *PRBS* excites the system by injecting in all 6 input channels a PRBS-9 sequence. This latter input, namely a Pseudo-Random Binary Signal (PRBS), is a deterministic signal with white-noise-like properties [29]. It is very well known in the experiment design field since it has the favourable property of equally distributing energy across all the frequencies in the input spectrum, thus allowing one to extract information of the models in different frequency ranges. Although not a common input in aircraft manoeuvres, it has been used in this spirit here, since the previously adopted sets of input will only give information on the behaviour of the reduced models around the aircraft reduced frequency ω_r. Results are shown in Fig. 5.

The plots confirm the advantage in using the BMD approach when seeking a low-order model capturing parameter variations. These results are important considering that are obtained by exploring a borader spectrum of the system's response than what was the case for purely sinusoidal inputs.

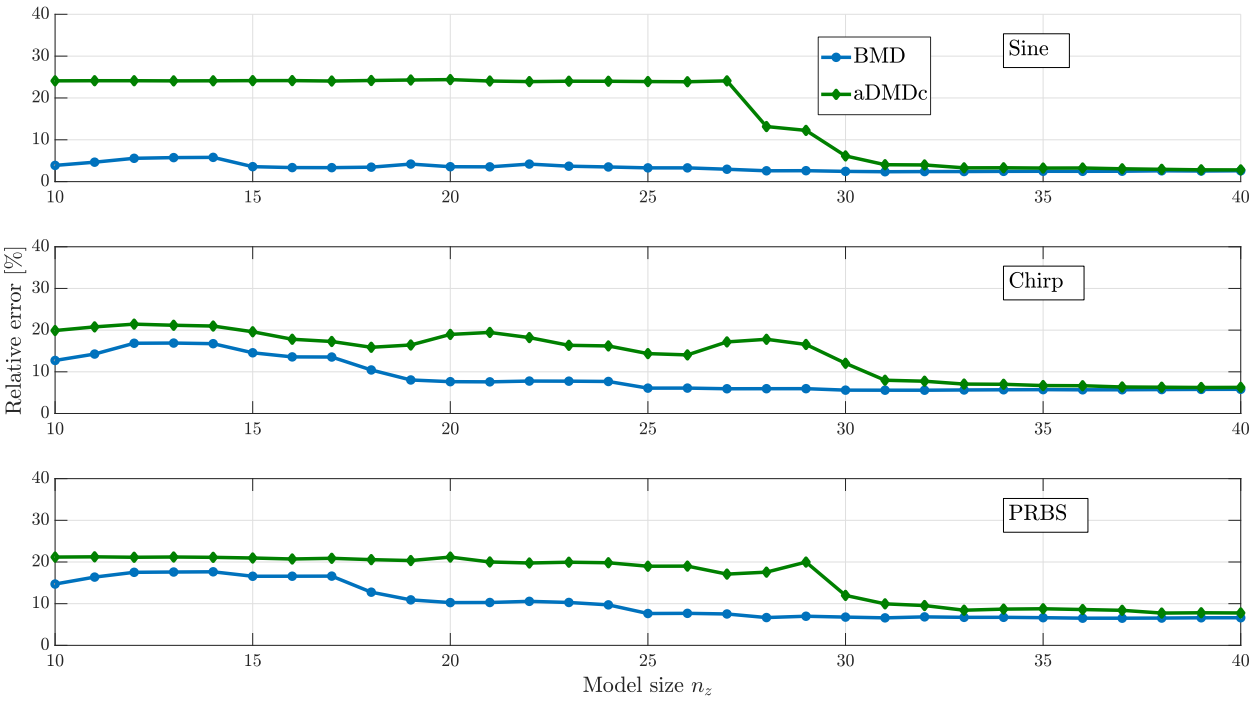

Fig. 5 Error on the prediction of the system's output (bending mode) for speed-varying manoeuvres with three different types of input signals.

V. Conclusion

The paper proposes the Balanced Mode Decomposition algorithm, a novel data-driven approach for constructing low-order LPV models from the system's trajectories. The main novelties compared to alternative approaches available in the literature are the use of an oblique projection (instead of an orthogonal one) and the projection onto subspaces defined based on controllability and observability properties of the system (rather than based on POD-type criteria). The performance of the BMD algorithm is assessed on a morphing wing for airborne wind energy applications by comparing it with the recently proposed aDMDc algorithm. The results, proposed both for the fixed parameter and for the parameter-varying case, confirm the theoretical advantages discussed in the technical part of the paper. Indeed, BMD achieves the lowest prediction error in the range of low order models. The improved accuracy is ascribed to the projection of the states onto a subspace that maximizes the information on the input-output content. Moreover, BMD provides a state consistency family of low-order LTI systems which gives a grid LPV model of the system, while still providing at the same time a parameter-varying projection operator.

Acknowledgments

This work is supported by the Swiss National Science Foundation under grant no. 200021_178890. The authors wish to thank Eva Ahbe for helpful discussions.

References

[1] Brunton, S. L., Noack, B. R., and Koumoutsakos, P., "Machine Learning for Fluid Mechanics," *Annual Review of Fluid Mechanics*, Vol. 1, No. 2, 2020, pp. 391–421.

[2] Schmid, P., "Dynamic mode decomposition of numerical and experimental data," *Journal of Fluid Mechanics*, Vol. 656, 2010, p. 5Ű28.

[3] Holmes, P., Lumley, J. L., Berkooz, G., and Rowley, C. W., *Turbulence, Coherent Structures, Dynamical Systems and Symmetry*, 2nd ed., Cambridge Monographs on Mechanics, Cambridge University Press, 2012. https://doi.org/10.1017/CBO9780511919701.

[4] Antoulas, A. C., *Approximation of Large-Scale Dynamical Systems*, Society for Industrial and Applied Mathematics, 2005.

[5] Proctor, J. L., Brunton, S. L., and Kutz, J. N., "Dynamic Mode Decomposition with Control," *SIAM Journal on Applied Dynamical Systems*, Vol. 15, No. 1, 2016, pp. 142–161.

[6] Toth, R., *Modeling and identification of linear parameter-varying systems*, Springer, 2010.

[7] Bennani, S., Willemsen, D. M. C., and Scherer, C. W., "Robust Control of Linear Parametrically Varying Systems with Bounded Rates," *Journal of Guidance, Control, and Dynamics*, Vol. 21, No. 6, 1998, pp. 916–922.

[8] Marcos, A., and Balas, G., "Development of Linear Parameter Varying Models for Aircraft," *Journal of Guidance, Control, and Dynamics*, Vol. 27, No. 2, 2004, pp. 218–228.

[9] Hjartarson, A., Seiler, P., and Packard, A., "LPVTools: A Toolbox for Modeling, Analysis, and Synthesis of Parameter Varying Control Systems," *1st IFAC Workshop on Linear Parameter Varying Systems LPVS*, Vol. 48, 2015, pp. 139–145.

[10] Varga, A., and Ossmann, D., "LPV model-based robust diagnosis of flight actuator faults," *Control Engineering Practice*, Vol. 31, 2014, pp. 135 – 147.

[11] Wang, Y., Song, H., Pant, K., Brenner, M. J., and Suh, P. M., "Model Order Reduction of Aeroservoelastic Model of Flexible Aircraft," *AIAA Scitech Forum*, 2016.

[12] Annoni, J., and Seiler, P., "A method to construct reduced-order parameter-varying models," *International Journal of Robust and Nonlinear Control*, Vol. 27, No. 4, 2017, pp. 582–597.

[13] Villemagne, C. D., and Skelton, R. E., "Model reductions using a projection formulation," *International Journal of Control*, Vol. 46, No. 6, 1987, pp. 2141–2169.

[14] van Overschee, P., and de Moor, L., *Subspace identification for linear systems: theory, implementation, applications*, Kluwer Academic Publishers, 1996.

[15] Theis, J., Seiler, P., and Werner, H., "LPV Model Order Reduction by Parameter-Varying Oblique Projection," *IEEE Transactions on Control Systems Technology*, Vol. 26, No. 3, 2018, pp. 773–784.

[16] Fonzi, N., Brunton, S. L., and Fasel, U., "Data-driven nonlinear aeroelastic models of morphing wings for control," *Proceedings of the Royal Society A: Mathematical, Physical and Engineering Sciences*, Vol. 476, No. 2239, 2020.

[17] Murua, J., Palacios, R., and Graham, J. M. R., "Applications of the unsteady vortex-lattice method in aircraft aeroelasticity and flight dynamics," *Progress in Aerospace Sciences*, Vol. 55, 2012, pp. 46 – 72.

[18] Fasel, U., Tiso, P., Keidel, D., Molinari, G., and Ermanni, P., "Reduced-Order Dynamic Model of a Morphing Airborne Wind Energy Aircraft," *AIAA Journal*, Vol. 57, No. 8, 2019, pp. 3586–3598.

[19] Fasel, U., Keidel, D., Molinari, G., and Ermanni, P., "Aeroservoelastic Optimization of Morphing Airborne Wind Energy Wings," *AIAA Scitech Forum*, 2019.

[20] Gavish, M., and Donoho, D. L., "The Optimal Hard Threshold for Singular Values is $4/\sqrt{3}$," *IEEE Transactions on Information Theory*, Vol. 60, No. 8, 2014, pp. 5040–5053.

[21] Tu, J. H., Rowley, C. W., Luchtenburg, D. N., Brunton, S. L., and Kutz, J. N., "On dynamic mode decomposition: Theory and applications," *Journal of Computational Dynamics*, Vol. 52, No. 1, 2014, pp. 477–508.

[22] Moore, B., "Principal component analysis in linear systems: Controllability, observability, and model reduction," *IEEE Transactions on Automatic Control*, Vol. 26, No. 1, 1981, pp. 17–32.

[23] Glover, K., "All optimal Hankel-norm approximations of linear multivariable systems and their L_∞-error bounds," *International Journal of Control*, Vol. 39, No. 6, 1984, pp. 1115–1193.

[24] Lall, S., Marsden, J. E., and Glavaški, S., "A subspace approach to balanced truncation for model reduction of nonlinear control systems," *International Journal of Robust and Nonlinear Control*, Vol. 12, No. 6, 2002, pp. 519–535.

[25] Seiler, P., Moore, R., Meissen, C., Arcak, M., and Packard, A., "Finite Horizon Robustness Analysis of LTV Systems Using Integral Quadratic Constraints," *Automatica*, Vol. 100, 2019, pp. 135–143.

[26] Iannelli, A., Seiler, P., and Marcos, A., "Worst-Case Disturbances for Time-Varying Systems with Application to Flexible Aircraft," *Journal of Guidance, Control, and Dynamics*, Vol. 42, No. 6, 2019, pp. 1261–1271.

[27] Keidel, D., Fasel, U., Baumann, L., Molinari, G., and Ermanni, P., "Experimental validation of a morphing wing for Airborne Wind Energy Applications," *8th International Conference on Adaptive Structures and Technologies*, 2017.

[28] Rodden, W. P., and Johnson, E. H., *User Guide V 68 MSC/NASTRAN Aeroelastic Analysis*, 1994.

[29] Ljung, L., *System Identification: Theory for the User*, Prentice Hall PTR, 1999.